UCRL-JC-129395
PREPRINT

Validation of a Ground Motion Synthesis and Prediction Methodology for the 1988, M=6.0, Saguenay Earthquake

Lawrence Hutchings, Steven Jarpe*, Paul Kasameyer, and William Foxall
Lawrence Livermore National Laboratory, Livermore, CA
*Institute for Crustal Studies, University of California, Santa Barbara, CA

This paper was prepared for submittal to
NCEER Workshop on Ground Motion Methodologies for the Eastern United States
Memphis, Tennessee
October 16 and 17, 1997

January 1998

Validation of a Ground Motion Synthesis and Prediction Methodology for the 1988, M=6.0, Saguenay Earthquake

Lawrence Hutchings, Steve Jarpe, Paul Kasameyer, and William Foxall

prepared for the NCEER Workshop on Ground Motion Methodologies for the Eastern United States

October 16 and 17, 1997

Lawrence Livermore National Laboratory
Earth Sciences Department
P.O. Box 808
Livermore, California 94551

Introduction

We model the 1988, M=6.0, Saguenay earthquake. We utilize an approach that has been developed to predict strong ground motion. This approach involves developing a set of rupture scenarios based upon bounds on rupture parameters. Rupture parameters include rupture geometry, hypocenter, rupture roughness, rupture velocity, healing velocity (rise times), slip distribution, asperity size and location, and slip vector. Scenario here refers to specific values of these parameters for an hypothesized earthquake. Synthetic strong ground-motions are then generated for each rupture scenario. A sufficient number of scenarios are run to span the variability in strong ground motion due to the source uncertainties. By having a suite of rupture scenarios of hazardous earthquakes for a fixed magnitude and identifying the hazard to the site from the one standard deviation value of engineering parameters we have introduced a probabilistic component to the deterministic hazard calculation. For this study we developed bounds on rupture scenarios from previous research on this earthquake. The time history closest to the observed ground motion was selected as the model for the Saguenay earthquake.

The approach is based on three hypotheses: 1) accurate computation of ground motions from a particular rupture scenario is possible, 2) a general description of the rupture is sufficient for engineering purposes; and 3) The rupture characteristics of a fault can be constrained in advance of possible future rupture by interpreting physical properties such as rheology, structure, lithology, seismicity, and tectonic slip along the fault. Corollaries to these hypotheses are that the range of possible fault rupture scenarios is narrow enough to functionally constrain the range of strong ground-motion predictions, and that a discrete set of rupture scenarios is sufficient, for engineering purposes, to span the infinite combinations possible from a given range of rupture parameters. Research to support these hypotheses is discussed below.

A realistic synthesis of ground motion should include the effects of geologic conditions along the propagation path from the fault and at the site itself. Geologic conditions can significantly alter the amplitudes of seismic energy, and can cause focusing and scattering of energy. Also, at sites close to large faults it is critical to account for the effects of finite fault rupture. These include seismic arrivals radiated from portions of the fault that can be tens of kilometers apart and arrive at the same time, and directivity effects that can significantly enhance or diminish amplitudes of the wave field. In addition, the superposition of direct and scattered body-waves and surface-waves will result in an extremely complicated wave field and should be modeled. To model all these affects we synthesize strong ground motion with physics based solutions of earthquake rupture that utilize empirical Green's functions and apply physically based rupture parameters.

We have developed an exact solution to the representation relation for finite rupture that utilizes either empirical or synthetic Green's functions (Hutchings and Wu, 1990; Hutchings 1991, 1994; Jarpe and Kasameyer, 1996). If the slip function is descretized as a summation of step functions and only frequencies below the sub-event corner frequency are considered, then the representation relation can be expressed as:

$$u_n(X, t) = \sum_{j=1}^{\eta} \kappa_j e_n(X, t' - \tau_j)_j \quad , \tag{1}$$

where e_n is the empirical Green's function, τ_j includes all time delays, and

$$\kappa_j = \frac{\mu_j A_j s_j}{M^e_{oj}} \quad , \tag{2}$$

with s_j calculated from the slip function. In our models κ varies according to the scenario described. If, for example, κ is constant that is equivalent to having a Haskell slip function with slip rate equal to rupture velocity. Derivations by Joyner and Boore (1986) are only applicable for this situation, at least for frequencies below the sub-event corner frequency.

Hutchings (1994) further pointed out that equation 2 can be used to develop a simple form of the Fourier amplitude spectra from synthesized seismograms. If it is assumed that the Fourier amplitude spectra at a particular site are similar, event though their phase spectra may be quite different, then the Fourier amplitude spectrum of the synthesized seismogram can be expressed as:

$$|U(\omega)| = |E(\omega)| \left\{ \sum_{j=1}^{\eta} \kappa_j^2 + \sum_{j=1}^{\eta} \sum_{\substack{k=1 \\ j \neq k}}^{\eta} \kappa_j \kappa_k \cos(\phi_j - \phi_k + \omega\tau_k - \omega\tau_j) \right\}^{\frac{1}{2}} \quad , \tag{3}$$

where, $\phi(\omega)$ is the phase spectrum of the empirical Green's functions.

The effect of different rupture parameters on the Fourier amplitude spectra is fairly easy to observe. At low frequencies, $\omega \to 0$ and the phase spectrum of different empirical Green's functions are the same, so spectral amplitudes are expressed as:

$$|U(\omega)| = |E(\omega)|\left(\frac{M_0}{M_0^e}\right). \tag{4}$$

Equation 4 gives the largest spectral amplitudes possible for the synthesized seismograms. Spectra at higher frequencies depend on the phase effects of different empirical Green's functions and on the delay times caused by rupture velocity and slip functions. The phase spectrum from empirical Green's functions located close to each other may be quite similar as is apparent by the similarity of their waveforms. Then, when $\tau_j \rightarrow \tau_k$ (such as in the case of a high rupture velocity and short rise time) large contributions to the spectra are included from the second summation at all frequencies and the spectrum approaches equation 4. As $\tau_j - \tau_k$ increases, such as from slow rupture velocity or longer rise times, only the first summation in equation 3 is significant and the spectrum approaches the smallest values possible.

In this study, we use recordings of small earthquakes to provide empirical Green's functions for frequencies 0.5 to 25.0 Hz, and analytical calculations to provide synthetic Green's functions for frequencies 0.05 to 0.5 Hz. We synthesize the entire wavetrain and for three components. Site soil can also significantly affect ground motions with non-linear effects, but here we only present linear ground motions that might be expected at a rock outcrop.

We model the rupture process as a continuous rupture over fault segments with variable slip amplitude. Areas of high slip are called asperities. This model is consistent, within the frequency range of resolution, with inversion studies (Wald et. al., 1990, 1993, 1995; Beroza and Spudich, 1988; Hartzel and Heaton, 1988; Hartzell 1989) and with what is known from dynamic rupture models about how earthquakes rupture (Rice, 1983; Kostrov and Das, 1988). However, these studies only resolve fault slip histories up to spatial resolutions of a couple of kilometers and frequencies up to one hertz. Nevertheless, our method provides good fits to observed seismograms up to 25 Hz when these models are used.

Green's Functions

The basic premise in synthesizing with empirical and synthetic Green's function is that each offers the best accuracy over particular frequency bands. Empirical Green's functions are defined here as recordings of effectively impulsive point source events (Hutchings and Wu, 1990). The empirical Green's functions have a better accuracy over high frequencies where geologic inhomogeneities are not well modeled, and the synthetic Green's functions have better accuracy over lower frequencies where empirical Green's functions do not have sufficient energy. The overlap is in the range from 0.5 to 1.0 Hz. In this range, the geology can be modeled with some accuracy and the empirical Green's function have sufficient energy to be well recorded.

We computed synthetic Green's functions using the reflectivity code of Kennett (1983). This solution extends to D.C., but does not include near-field terms. Focal mechanism radiation pattern is used for synthetic Green's functions solutions to the finite rupture. We only considered solution for frequencies greater than 0.05 Hz (20 sec period), as lack of near-filed arrivals diminish the reliability of solutions for frequencies lower than this. The velocity model is listed below.

Empirical Green's functions should be recorded at the site of interest and from source events along the faults of interest, since site response and near source propagation path effects are highly variable. Empirical Green's functions include the actual effects of velocity structure, attenuation, and geometrical spreading. In this study empirical Green's functions were not available from the sites to be modeled. We used recordings of small earthquake from nearby weak-motion recorders to obtain empirical Green's functions. These were interpolated to have been located from the sites for modeling. Note, the location for each egf in the sources file is one of a group of pre-defined points that are in "the vicinity" of our fault. The way the point is chosen is it is the same distance from the strong motion station as the distance from the weak motion recording station was to the weak motion event. In some cases, different recordings are put at the same location because their recorded distances are similar.

It is not possible to record empirical Green's functions from all locations along a fault of interest and with the same focal mechanism solution, so that source locations of empirical Green's functions have also been interpolated to fill in the fault. The spatial dependence of empirical Green's functions has been researched by Hutchings and Wu (1990) and they found that the variability in ground motion due to differences in source location and/or focal mechanism solutions are much less than that due to the site response, and Hutchings (1991), Hutchings (1994), and Jarpe and Kasameyer (1996) found that interpolation for different source locations along a fault works quite well. Also, it is not necessary to have source events fall directly along the fault of interest, but to be located near the fault. In synthesis, we have the option of correcting for different focal mechanism solutions, but Hutchings and Wu (1990) and Jarpe and Kasameyer (1996) found that for high frequencies it does not improve the synthesis. Interpolation is performed by correcting for attenuation, 1/R, and P- and S-wave arrival times due to differences in source distance. We include the radiation pattern effect for low frequencies, when we use synthetic Green's functions.

Weak Motion Stations:

A11 47.24250 -70.19780

A16 47.47060 -70.00640

A21 47.70360 -69.68970

A54 47.45670 -70.41250

A61 47.69300 -70.09000

A64 47.82640 -69.89220

Source Events

yymmddhhmmss lat lon dep mag

970902142120 47.62 -70.01 27.1 1.7

970902191234 47.43 -70.17 14.0 1.3

970903133907 47.55 -70.29 10.5 1.2

970903155227 47.47 -70.06 8.8 2.5

970903230612 47.53 -69.89 13.0 2.4

970904071841 47.54 -69.89 13.5 1.5

970906090800 47.63 -69.87 15.0 1.6

970909182049 47.37 -70.41 7.9 2.5

970909214848 47.46 -70.03 12.7 1.0

970910012327 47.56 -70.35 4.7 2.0

970921005233 47.67 -69.8 11.4 1.4

970924171312 47.75 -69.91 22.8 2.2

970928133434 46.92 -71.37 18.0 1.3

We compared our moment calculations based upon our moment-magnitude relation to moments calculated by Haddon (1995) for 5 aftershocks of the Saguenay earthquake. I used our moment-magnitude relation with his Mblg magnitudes and compared them to his moment calculations. Our magnitudes are listed as Ml, so this may account for the difference. Our moment magnitude relation: Mo = 10**(1.2Ml - 17.0).

Saguenay Mblg	Haddon moment	Our relation	factor
6.5	7.9x10**24	1.2x10**24	0.15
4.8	3.2x10**22	5.8x10**22	1.8
4.1	1.4x10**21	8.3x10**21	5.9
2.9	6.3x10**19	3.0x10**20	4.8
2.8	6.3x10**19	2.3x10**20	3.7
2.6	6.3x10**19	1.3x10**20	2.1

If our moments are systematically a factor of 3.5 too large, then the amplitudes of the high frequency is synthetic seismograms (>2.0 Hz) would be systematically increased by a factor of 3.6. This should be researched.

Validation

Jarpe and Kasameyer (1996) constrained the rupture history of the 1989 Loma Prieta earthquake using rupture parameters from independent studies to compute broadband synthetic seismograms at 26 strong motion sites that recorded the earthquake. They characterized the earthquake source in terms of rupture parameters used in this study. They obtained very good fits to the observed time histories, spectra, and computed engineering parameters. They found that the errors between computed and observed response spectra were less than or equal to those from other methods for periods in the range of 0.05 to 0.4 s. Between 0.5 and 2.0 s, the errors were significantly less than those from methods based on regression of recorded strong motion data. From these studies Jarpe and Kasameyer established random and model errors for this method.

Hutchings (1994) carried out a more extensive investigation of rupture models and found that nearly exact synthesis of small earthquake seismograms can be achieved when the same set of parameters is independently constrained. Hutchings also obtained good fits to observed accelerograms recorded from the 1971 San Fernando earthquake using similar simple rupture models. Hutchins et al. (1997) also modeled the Ms=6.7 24 February 1981, Corinth, central Greece earthquake with source parameters fixed from previous studies and found a good match to observed seismograms. These validations support hypotheses 1 and 3 above.

Foxall et al. (1995) used the approach outlined in this study to predict the ground motion from the Loma Prieta earthquake. They developed bounds on the same rupture parameters described below and predicted ground-motion hazard at 26 sites where strong ground motions were recorded. They generated a suite of synthesized seismograms at each site, and calculate log-normal average and one standard deviation values of peak acceleration, pseudo-velocity response spectra, and Fourier amplitude spectra. This established the parametric uncertainty in the study. they also added the random and modeling error obtained from the Jarpe and Kasameyer study for the Loma Prieta earthquake. Foxall et al. successfully predicted the hazard at 23 of 26 sites within the 16 and 84% confidence levels of these engineering parameters.

The Foxall et al study supports hypothesis 3 above. They point out that imaging the lithology of the fault zone can provide information on geometry and location of asperities, rupture velocities, and source rise times; and improves interpretation of the slip and seismicity data. Interpretation of seismicity data and tectontic slip rates can provide information on geometry and location of a potential rupture zones and asperities. Interpretation of geology and geologic structure can provide information on geometry of rupture and rupture velocities. Geometrical irregularities of structure and fault traces, such as steps and bends, can be interpreted to obtain fault segmentation boundaries. Finally, dynamic, kinematic, and laboratory modeling of rupture provides pertinent information on rupture velocity, hypocenter locations, rise times, and slip functions.

Source Description

Here we outline the source parameters used in the synthesis. They are obtained from previous studies. Generally, we used previous studies to provide bounds on fault rupture parameters, or the average value to provide fixed values when necessary.

Moment

The chosen is 7.0 $x10^{24}$ dyne-cm, which is the average of studies listed in Table 1.

Table 1:

moment	reference
$8x10^{24}$	North *et al.*, 1989
$6.3x10^{24}$	Boore and Atkinson, 1992
$8.9x10^{24}$	Boatwright and Choy, 1992
$6.9x10^{24}$	Haddon, 1995
$5.0x10^{24}$	Sommerville et al., 1990
	Cabajal and Barker, 1992
$7.0x10^{24}$	this study

Geometry

The geometry is a rectangular rupture with width that varies from 1.5 to 3.5 km and length that varies from 8 to 12 km. Therefore the rupture area ranges from 12 - 42 km^2. This is consistent with the range found in studies listed in Table 2. We chose a fixed point on the fault at 48.117N 71.184W, and allowed the fault length in direction of strike to vary from 2 to 4 km, and the length in the negative strike direction to vary from 6 to 8 km. the with varied from 1.5 to 3.5 km, and the top of fault rupture varied from 26 to 30 km. The fixed point is consistent with the hypocenter and the along and negative strike distances for the fault are consistent with Haddon (1992) and Beresnev and Atkinson (1997) (Table 2). the geometry that provided the best fit to observed strong ground motion is listed in Table 2.

Table 2:

shape	dimensions	Area	
rectangular	2x14km	$28km^2$	Beresnev and Atkinson, 1997
circular	2.5km radius	19.6	Somerville et al., 1990
elliptical		15	Haddon 1995
rectangular	2.1x8.4	17.6	this study

Focal Mechanism Solution

The center value of the focal mechanism solution used in this study is the average of previous studies (Table 3): strike N325°E; dip 65°E; slip rake -65°. Focal mechanism descriptions are described by the convention of Aki and Richards (1980): dip is down to right of strike, with positive slip vector for reverse faulting. We held the strike fixed and allowed the dip and slip vector to vary by +/- 10°. The focal mechanism of the scenario that provided the best fit to observed seismograms is listed in Table 3.

Table 3:

Strike	Dip	Slip Vector	Author
326°	67°	-54°	North *et al.*, 1989
320°	65°	-78°	Somerville *et al.*, 1990
325°	74°	-50°	Carabajal and Barker, 1989
328°	51°	-70°	Haddon, 1995
340°	63°	-90°	NEIC
317°	64°	-60°	HARVARD
325°	63°	-70°	this study

Crustal Model

The crustal velocity model is used for calculating synthetic Green's functions is from Haddon (1995) and is listed in Table 4. Program EMPSYN utilizes a linearly increasing velocity model that approximates the model listed to determine rupture and healing velocity during rupture and for interpolation of empirical Green's functions. The velocity model is approximated by:

Vp = 6.0 + 0.02Z, and Vp = 8.0 at 45.0 km; where Z is depth.

Table 4:

D (km)	H (km)	α (km/sec)	β (km/sec)	ρ (gm/cm^3)
0.0 - 37.0	37.0	6.50	3.65	2.70
37.0 - 45.0	8.0	6.85	3.95	2.85
> 45.0		8.00	4.65	3.30

Strong Motion Data

Haddon (1995) estimated the low frequency cutoff of reliability of the recorded strong motion data, these are listed in Table 2.

Table 5:

Strong motion stations	station location	frequenc range Hz
SM01	48.123 71.123	0.7-25.0
SM02	46.778 70.275	1.0-25.0
SM05	48.143 69.719	0.4-25.0
SM08	47.655 70.153	0.5-25.0
SM09	47.426 69.805	0.5-25.0
SM10	47.476 69.996	0.5-25.0
SM16	48.490 71.012	1.0-25.0

Table 5:

Strong motion stations	station location	frequenc range Hz
SM17	48.325 71.992	1.0-25.0
SM20	47.550 70.327	0.5-25.0

In synthesizing seismograms, synthetic seismograms were used from frequencies 0.05 to 2.0 Hz, and empirical Green's functions were used for frequencies 2.0 to 50.0 Hz.

Rupture Models

Our earthquake rupture models rely on moment, fault geometry, hypocenter, rupture roughness, rupture velocity, healing velocity, slip vector, and asperity location. Moment and fault geometry (extend of rupture and its orientation) are held fixed, while the other parameters were allowed to vary within limits. The fault was descritized into 0.01 Km^2 elemental areas, which are small enough that modeled rupture is continuous for frequencies up to 25.0 Hz.

The rupture initiates at the hypocenter and propagates radially at a percentage of the shear wave velocity. Slip at a point obtains the amplitude of the Kostrov slip function, but the shape is approximated as a ramp. We have arbitrarily limited the rupture propagation factor in the Kostrov slip function to be equal to or less than the rupture time to the closest fault edge from the hypocenter. To develop scenarios, we used a computer program that randomly varies rupture parameters within prescribed constraints. The parameter constraints for rupture scenarios are listed in Table 1 and their bounds are as follows:

ASPERITIES were included to add high slip amplitudes to portions of the rupture. Asperities are circular and have a diameter randomly chosen to be between 0.2 and 0.8 times the fault width. The number of asperities is randomly selected for each scenario. Stress drop in asperity portions of rupture are higher than other portions of the rupture area.

ROUGHNESS is simulated as elements resisting rupture, then breaking. A percentage of elements (0, 10, 20, 33, or 50%) have a shortened rise time of between 0.1 and 0.9 times neighboring elements, but with rupture completed at the same time as neighboring elements. These rough elements have corresponding high stress drop.

HYPOCENTER was constrained to occur at least 0.1 kilometer from the fault edges.

RUPTURE VELOCITY is randomly selected to be from 0.75 to 1.0 times the shear wave velocity.

HEALING VELOCITY is the velocity for the phase that travels from a fault boundary to terminate slip. The free surface is not allowed to be a healing boundary for rupture since significant seismic pulses that are necessary shut down slip (Das and Kostrov, 1988; Schultz, 1989) are not generated from the surface (discussed below). The healing velocity is randomly selected to be between 0.8 and 1.0 times the shear-wave velocity. This is the range from the Rayleigh to shear wave velocity.

RISE TIME is equal to the time after the initiation of rupture for the first healing phase, initiated after the rupture front arrives any fault edge, to arrive.

STRESS DROP is a dependent variable derived from the Kostrov slip function and allowed to vary due to two effects modeled in rupture. First, asperities are allowed to have a different stress drop than surrounding portions of the fault rupture. Second. stress drop is constrained to diminish near the surface of the earth at the rate of 10 + 0.75 x the confining pressure due to the lithostatic load (300 bars at 1.7 km depth). The minimum of this and the full rupture stress drop is used.

SLIP VECTOR is constrained to 180^{o} for a right-lateral strike slip fault.

Prediction Uncertainty

We assume that the rupture scenarios are all of equal probability and that spectral values of their synthesized ground motions are log-normally distributed. Figures 3 and 4 show 36 absolute acceleration response (AAR) spectra (average of the log of the two horizontal components) obtained from the time histories at stations SM16 and SM17.

Also shown is Figures 3 and 4 are the median and one standard deviation values for prediction uncertainty for the one hundred AAR spectra at Stations S16 and SM17 along with the observed values. Uncertainty is estimated from (in the terminology used by Abrahamson et al.,1990) (1) parametric uncertainty, from not knowing which scenario will occur. This is estimated from the one standard deviation value obtained from running many rupture scenarios. (2) random and modeling errors due to moment estimates for source events, interpolating empirical Green's functions, and in not modeling the actual rupture process correctly was estimated by Jarpe and Kasameyer (1996) for 26 sites that recorded the Loma Prieta earthquake. This error is unknown for the sites in this study, but is assumed to be equal to their one standard deviation value. Prediction uncertainties are added in quadrature.

Results

For this study we ran 36 scenarios at two sites (SM16 and SM17) to choose possible model.s. From these two site we chose 5 scenarios to run at all sites to choose the best model. Figure shows the geometry of the preferred fault model geometry. Asperity locations are shown. Slip distribution contour are not shown. Asperity sizes are:

Asperity	maximum disp	radius	moment x10^{24}
SAG04_asper.01	220.4	0.6	0.008
SAG04_asper.02	202.1	0.7	0.010
SAG04_asper.03	129.4	0.3	0.001
SAG04_asper.04	297.7	0.2	0.001

Source propterities:

Properities of the selected source model scenario:

Mo = 7.0×10^{24} dyne-cm

focal mechanism solution: stk N325°E, dip 63°E, slip vector rake -70°(normal-left-lateral)

rupture area: 2.1 x 8.4km

top of rupture: 29.6 km

hypocenter: 48.102°N 78.105°W H=30.9

maximum slip: 526 cm

maximum rise time: 0.64 s

average slip: 132 cm

source duration: 1.53 s

stress drop: 387 bars

Figures 6-14 show comparisons of the observed to synthesized seismograms. The left column of each figure is the acceleration of the observed with the synthesized below for each component. Observed records are aligned with the S -waves of the synthesized records. Synthesiz4d records are plotted relative to origin time. Records are band pased to the frequency range of observation available for the observed records listed in Table 5. columns two and three are the integrated records (an multiplied by 980 cm/sec) to velocity (cm/sec) and displacement (cm). The top two boxes to the right of each figure is the Fourier amplitude spectra of each horizontal component, and the bottom right shows the absolute acceleration response.

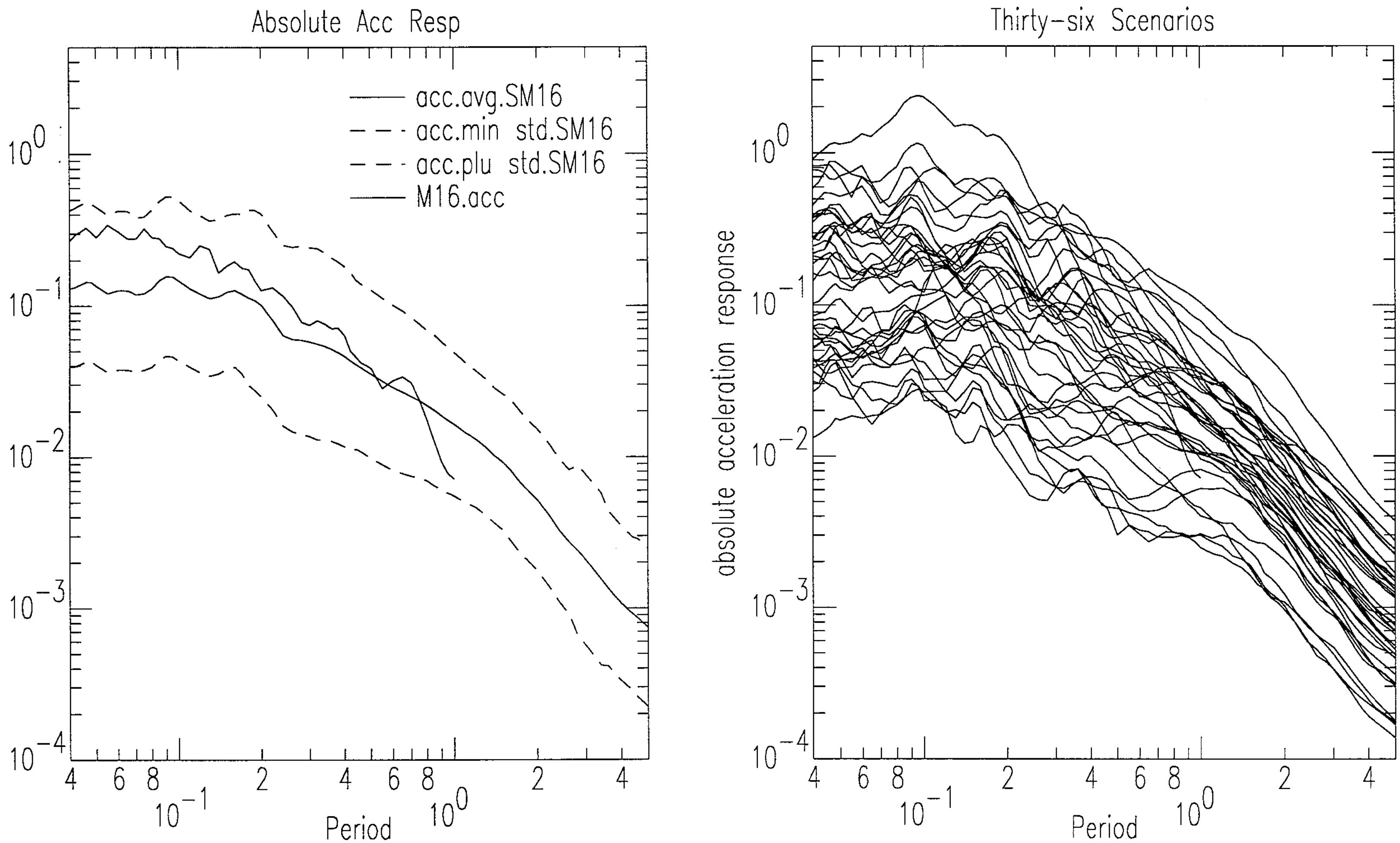
Absolute Acc Resp
acc.avg.SM16
acc.min std.SM16
acc.plu std.SM16
M16.acc
10^0
10^-1
10^-2
10^-3
10^-4
4 6 8 10^-1 2 4 6 8 10^0 2 4
Period
Thirty-six Scenarios
absolute acceleration response
10^0
10^-1
10^-2
10^-3
10^-4
4 6 8 10^-1 2 4 6 8 10^0 2 4
Period

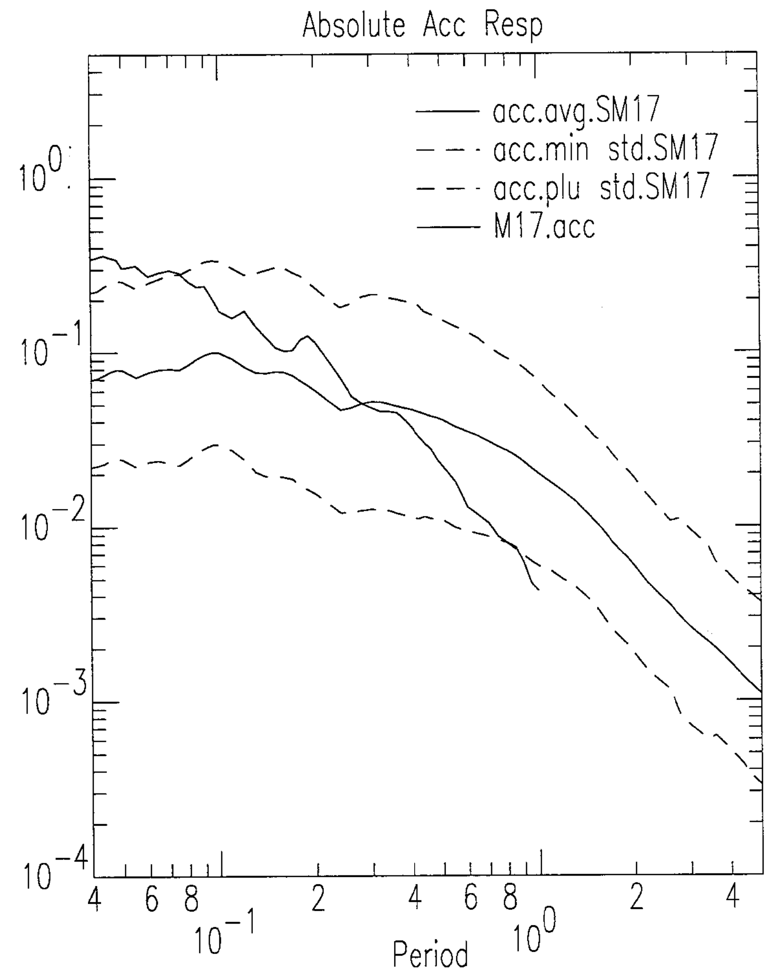
Absolute Acc Resp
acc.avg.SM17
acc.min std.SM17
acc.plu std.SM17
M17.acc
10^0
10^{-1}
10^{-2}
10^{-3}
10^{-4}
4 6 8 2 4 6 8 2 4
10^{-1}
Period
10^0

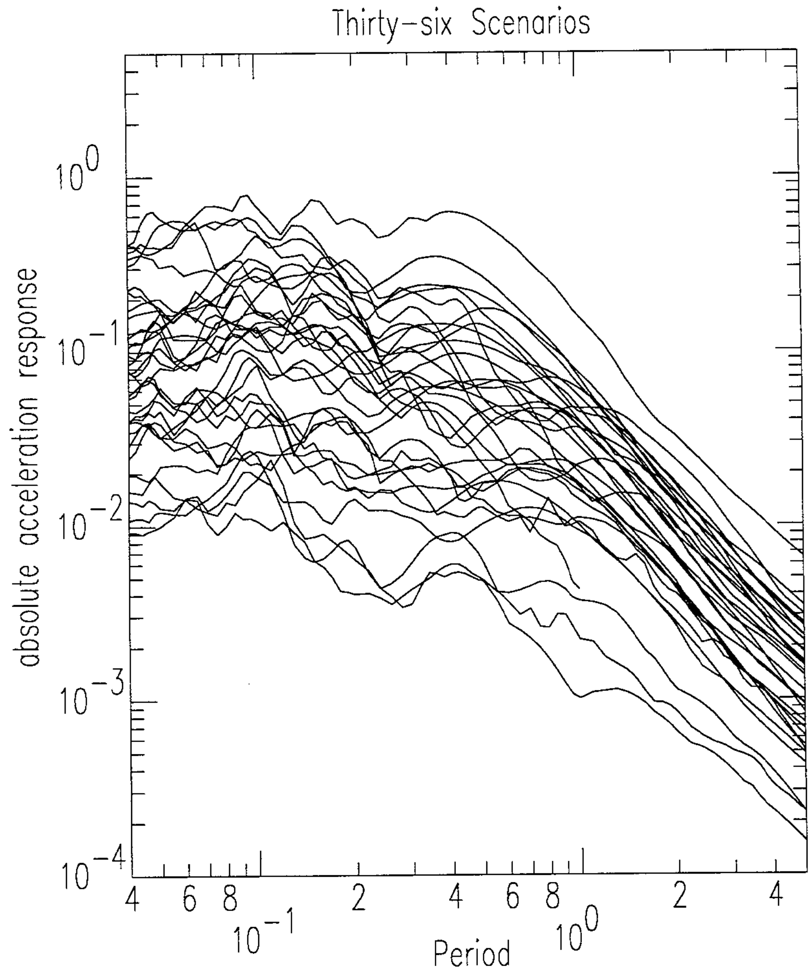
Thirty-six Scenarios
absolute acceleration response
10^0
10^{-1}
10^{-2}
10^{-3}
10^{-4}
4 6 8 2 4 6 8 2 4
10^{-1}
Period
10^0

References

Abrahamson, N. A., P. G. Somerville, and C. A. Cornell (1990), *Uncertainity in Numerical Strong Motion Predictions*, in *Proc. 4th U.S. National Conf. Earthquake Engineering*, Vol. 1 (Earthquake Engineering Research Institute, 20–24 May, Palm Springs, California).

Aki, K., and K. Irikura (1991). Characterization and mapping of earthquake shaking for seismic zonation, in *Proceedings of the Fourth International Conference on Seismic Zonation, Vol. I*, EERI, Oakland, 61-110.

Aki, K., and P. G. Richards (1980), *Quantitative Seismology, Theory and Methods*, Volumes I and II (W. H. Freeman and Company, San Francisco, CA).

Beresnev, I.A. and G.M. Atkinson (1997) Modeling finite-fault radiation from the ω^2 spectrum. *Bul. Seis. Soc. Am.* **87**, pp 67-84.

Beroza, G.C. and P. Spudich (1988) Linearized inversion for fault rupture behavior: application to the 1984 Morgan Hill, California earthquake. *J. Geophys. Res.* **93** 6275-6296.

Boatwright, J. and G.L. Choy (1992) Acceleration source spectra anticipated for large earthquakes in northeastern North America. *Bull. Seis. Soc. Am.* **82**, 660-682.

Boatwright, J. (1988). The seismic radiation from composite models of faulting, *Bul. Seis. Soc. Am.* **78**, 489–508.

Boore, D.M. and G.M. Atkinson (1987) Source spectra for the 1988 Saguenay earthquakes. *Bull. Seis. Soc. Am.* **82,** 683-719.

Carabajal, C.C. and J.S. Barker (1991) Source processes and wave propagation effects of the November 25, 1988 Saguenay, Quebec earthquake. abstract, *EOS* 72, 202.

Das, S., and B. V. Kostrov (1985), *An Elliptical Asperity in Shear: Fracture Process and Seismic Radiation*, Geophys. J. Roy. Astron. Soc. *80*, 725–742.

Foxall, William (1992) Heterodeneous Slip and Rupture Models of the San Andreas Fault Zone based upon Three-Dimensional Earthquake Tomography. dissertation, University of California, Berkeley, pp.168.

Foxall, William, Lawrence Hutchings, and Paul Kasameyer (1995) Lithological and Rheological Constraints on Fault Rupture Scenarios for Ground Motion Hazard Prediction. *IUTM Symposium on Mechanics Problems in Geodynamics*, Sept. 5-9, 1994, Beijing, China; UCRL-JC 116437 Lawrence Livermore National Laboratory, pp 27. submitted to *Bul. Seis. Soc. Am.*

Haddon, R.A.W. (1995) Modeling of source rupture characteristics for the Saguenay earthquake of November 1988. *Bull. Seis. Soc. Am.* **85**, 525-551.

Haddon, R.A.W. (1996) Use of empirical Green's functions, spectral ratios, and kinematic source models for simulatijng strong ground motion. *Bull. Seis. Soc. Am.* **86,** 597-615.

Haddon, R.A.W. (1992) Waveform modeling of strong motion data for the Saguenay earthquake of 25th November, 1988. *Bull. Seis. Soc. Am.* **82,** 720-754.

Hanks, T.C. and H. Kanamori (1979) A moment magnitude scale. *J. Geophys. Res.* **84,** 2348–2350.

Heaton, T. H. (1982). The 1971 San Fernando earthquake: a double event? *Bul. Seis. Soc. Am.* **72,** 2037–2062.

Hutchings, L. (1988). Modeling strong earthquake ground motion with an earthquake simulation program EMPSYN that utilizes empirical Green's functions, Lawrence Livermore National Laboratory, Livermore, CA, *UCRL-ID-105890*, p. 122.

Hutchings, L. (1991). "Prediction" of strong ground motion for the 1989 Loma Prieta earthquake using empirical Green's functions, *Bul. Seis. Soc. Am.* **81**, 88–121.

Hutchings, L. (1994) Kinematic Earthquake Models and Synthesized Ground Motion Using Empirical Green's Functions. *Bul. Seis. Soc. Am.* **84**, pp. 1028-1050.

Hutchings, L. and F. Wu (1990). Empirical Green's functions from small earthquakes—A waveform study of locally recorded aftershocks of the San Fernando earthquake, *J. Geophys. Res.* **95**, 1187–1214.

Hutchings, L. and S. Jarpe (1995) Ground motion Variability at the Highways 14 and I-5 Interchange in the Northern San Fernando Valley. in press *Bul Seis Soc Am.*

Hutchings, L., E. Ioannidou, S.P. Jarpe, G.N. Stavrakakis, and P. Kasameyer. Strong Ground Motion Synthesis for a M=7.2 earthquake in the Gulf of Corinth, Greece using Empirical Green's functions, presented, 29th IASPEI General Assembly, Thessaloniki, Greece, August 18-28,1997

Irikura, K. (1983). Semi-empirical estimation of strong ground motions during large earthquakes. *Bull. Disaster Res. Inst.*, Kyoto Univ., 33, 63-104.

Jarpe, S.P. and P.W. Kasameyer (1995). Validation of a Methodology for Predicting Broadband Strong Motion Time Histories from Empirical Green's Functions. in press, *Bul. Seis. Soc. Am.*

Joyner, W. B. and D. M. Boore (1986). On simulating large earthquakes by Green's-function addition of smaller earthquakes, *Earthquake Source Mechanics,* Geophysical Monograph No. 37, Maurice Ewing, Ed., **8**, 269–274.

Kennett, B. L. N. (1983) *Seismic Wave Propagation in Stratified Media,* Cambridge University Press, Cambridge.

Kostrov, B.V. and S. Das (1988) Principles of earthquake source mechanics, in *Cambridge Monographs on Mechanics and Applied Mathematics*, Cambridge University Press, Cambridge.

McCallen, D.B., K.M. Romstad, and G.L. Goudreau (1992) *Dynamic Response of a Reinforced Concrete Box-Girder Bridge.* Lawrence Livermore National Laboratory, Livermore, California, *UCRL-53868-91*, pp 2-12.

McCallen, D.B. and L.J. Hutchings (1995) Ground motion estimation and nonlinear seismic analysis. LLNL, UCRL-JC-121667. in press, proceedings: 12th Conference on Analysis and Computation of the American Society of Civil Engineers, Chicago, Illinois, 1986.

North, R.G., R.J. Wetmiller, J.E. Adams, F.M. Anglin, H.S. Hasegawa, M. Lamontagne, R. Du Berger, L. Seeber, and J. Armbruster (1989) Preliminary results from the November 25, 1988 Sagueny (Quebec) earthquake. Geophys. Res. Lett. **60**, 89-93.

Papageorgiou, A.S. and K. Aki (1983). A specific Barrier model for the Quantitative description of inhomogeneous faulting and the prediction of strong ground motion. I. Description of the model. *Bul. Seis. Soc. Am.* **73**, 693–722.

Rice, J.R. and A.L. Ruina (1983) Stability of steady friction slipping. *J. Appl. Mech.*, **105**, 343-349.

Scholz, C.H. (1990) *The mechanics of Earthquake Faulting*, Cambridge University Press, Cambridge, 439p.

Somerville, P.G., J. McLaren, C. Saikia, and D. Helmberger (1990). The Nov. 25, 1988 Saguenay, Quebec earthquake: source parameters and the attenuation of strong ground motion. *Bull. Seis. Soc. Am.* **80**, 1118-1143.

Tumarkin, A.G., R.J. Archuleta, and R. Madariaga (1994) Basic scaling relations for composite models, *Bull. Seism. Soc. Am.* **84**, no 4.

Wald, D.J., D.V. Helmberger and S.H. Hartzell (1990) Rupture process of the 1987 Superstition Hills Earthquake from inversion of Strong-Moyion Data. *Bul. Seis. Soc. Am.* **80**, 1079–1098.

Wald, D. J., T. H. Heaton, and K.W. Hudnut (1995) The Slip History of the 1994 Northridge, California Earthquake Determined from Strong -Motion, Teleseismic, GPS, and Leveling Data. preprint, *Bul. Seism. Soc. Am.* **81** (1).

Wald, David J., Donald V. Helmberger, and Thomas H. Heaton (1991) Rupture Model of the 1989 Loma Prieta Earthquake from Inversion of Strong-Motion and Broadband Teleseismic Data. *Bul. Seis. Soc. Am.* **81**, 1540–1572.

Wennerberg, L. (1990). Stochastic summation of empirical Green's functions, *Bul. Seis. Soc. Am.* **80**, 1418–1432.

Working Group on California Earthquake Peobabilities (1990) Probabilities of Large Earthquakes in the San Francisco Bay Region, California. U.S. Geological Survey Circular 1053.

Working Group on California Earthquake Peobabilities (1988) Probabilities of Large Earthquakes Occurring in California on the San Andreas Fault. U.S. Geological Survey Open-file Report 88-398.

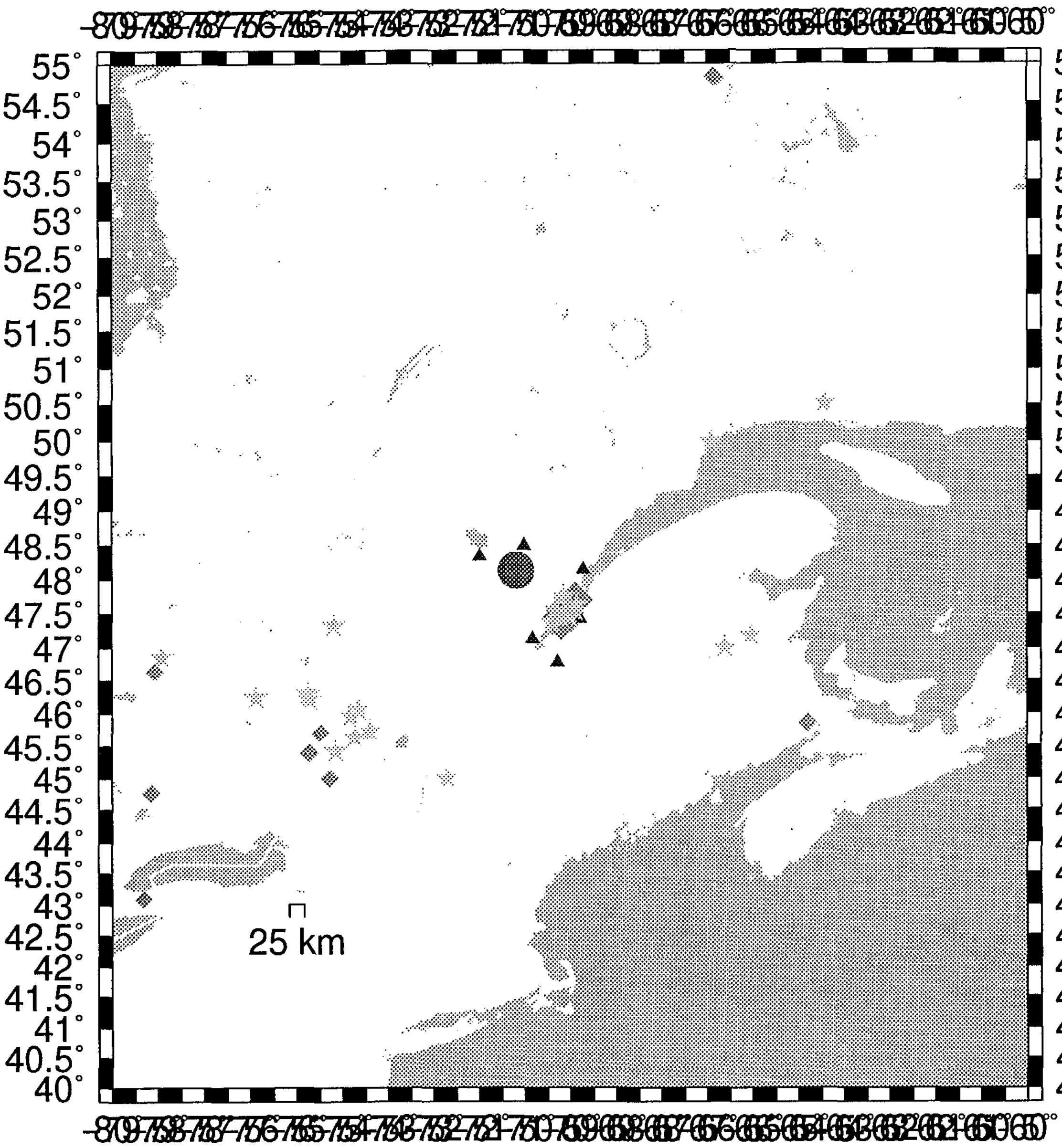

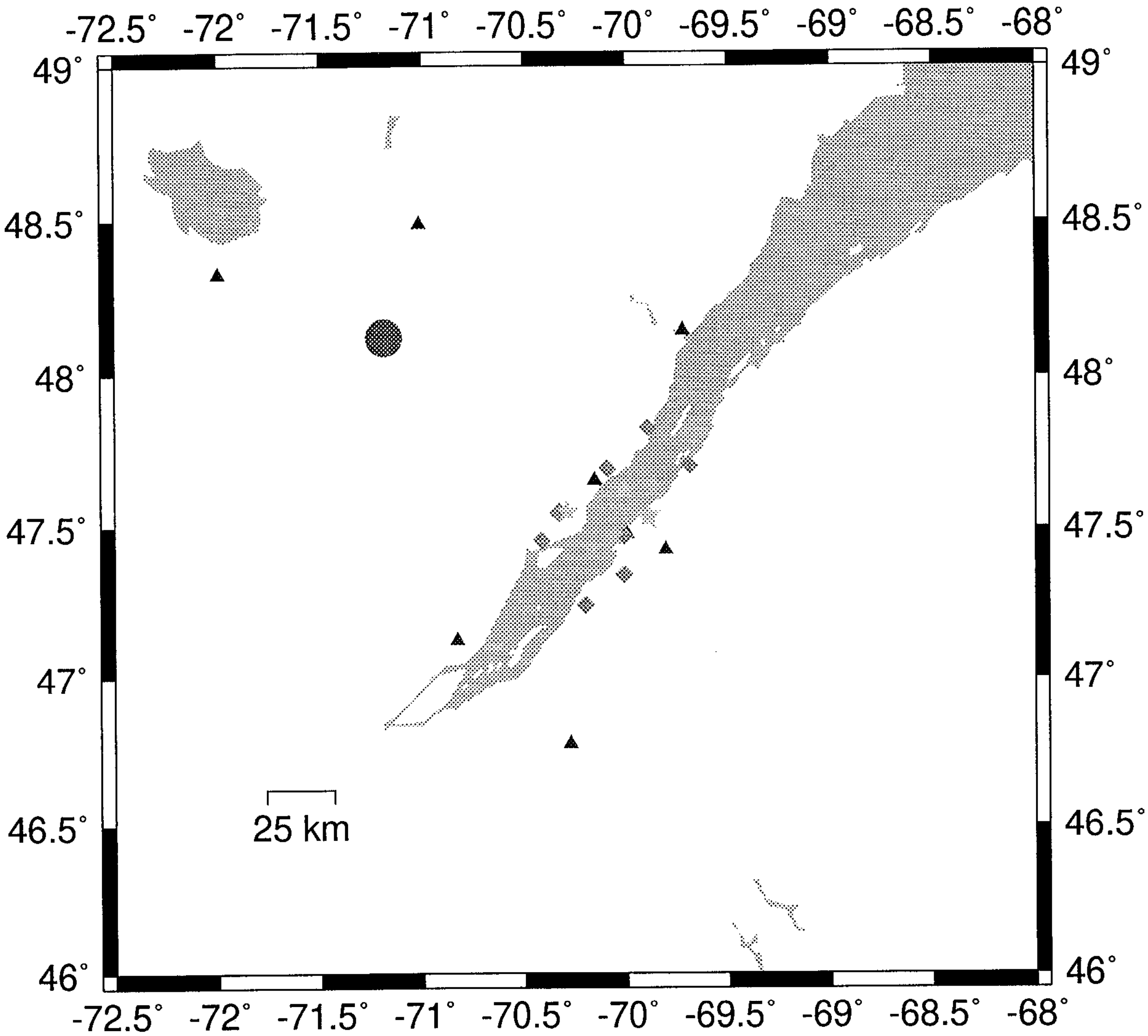
-72.5° -72° -71.5° -71° -70.5° -70° -69.5° -69° -68.5° -68°
49°
48.5°
48°
47.5°
47°
46.5°
46°
25 km

SAG01	none	h 20 .070	48.109	-71.168	30.32	325.0	71.0	69.2	0.97	0.87	0.01
SAG02	01,02,03,04,05	h 10 .041,.003,.014,.004,.004,.004	48.081	-71.142	29.86	325.0	72.1	66.2	0.83	0.91	0.01
SAG03	01,02,03	h 50 .043,.001,.014,.012	48.137	-71.190	30.47	325.0	59.0	57.6	0.90	0.87	0.01
SAG04	01,02,03,04	h 20 .050,.008,.010,.001,.001	48.104	-71.155	30.86	325.0	63.4	70.4	0.86	0.98	0.01
SAG05	01	h 20 .066,.004	48.121	-71.173	30.29	325.0	55.5	55.1	0.98	0.99	0.01
SAG06	01	h 0 .056,.014	48.130	-71.181	30.82	325.0	61.9	60.8	0.82	0.96	0.01
SAG07	01,02	h 50 .054,.005,.011	48.077	-71.141	29.19	325.0	65.7	65.1	0.86	0.94	0.01
SAG08	01,02,03	h 25 .055,.001,.004,.010	48.107	-71.175	28.78	325.0	67.9	61.6	0.86	0.96	0.01
SAG09	01,02,03	h 25 .048,.018,.002,.002	48.102	-71.149	31.13	325.0	62.2	66.0	0.99	1.00	0.01
SAG10	01	h 33 .065,.005	48.097	-71.166	28.59	325.0	63.3	67.4	0.98	0.97	0.01
SAG11	01,02,03	h 20 .030,.018,.013,.009	48.133	-71.201	28.95	325.0	58.2	59.2	0.95	0.93	0.01
SAG12	01,02	h 33 .054,.002,.014	48.118	-71.176	30.17	325.0	65.9	74.1	0.83	0.83	0.01
SAG13	01,02,03,04	h 10 .017,.004,.014,.006,.029	48.122	-71.173	31.36	325.0	66.8	57.0	0.93	0.88	0.01
SAG14	01,02	h 20 .065,.001,.005	48.074	-71.142	28.58	325.0	70.8	66.0	0.86	0.81	0.01
SAG15	01,02,03,04	h 10 .026,.006,.006,.025,.007	48.076	-71.132	30.46	325.0	70.8	68.2	0.84	0.99	0.01
SAG16	01,02,03	h 33 .058,.003,.001,.007	48.111	-71.185	27.64	325.0	71.1	58.0	0.76	0.85	0.01
SAG17	01	h 25 .069,.001	48.091	-71.164	28.01	325.0	65.6	70.9	0.77	0.90	0.01
SAG18	01	h 20 .064,.006	48.076	-71.139	29.39	325.0	73.2	58.7	0.78	0.82	0.01
SAG19	01,02,03	h 50 .060,.003,.001,.006	48.075	-71.144	28.10	325.0	74.8	58.1	0.87	0.86	0.01
SAG20	01,02,03,04	h 25 .056,.010,.001,.001,.002	48.089	-71.148	29.72	325.0	59.9	68.2	0.97	0.85	0.01
SAG21	none	h 0 .070	48.094	-71.158	29.39	325.0	74.4	56.0	0.99	0.91	0.01
SAG22	01,02	h 50 .067,.001,.001	48.121	-71.178	30.42	325.0	65.6	72.4	0.99	0.86	0.01
SAG23	01,02,03	h 10 .065,.001,.002,.002	48.104	-71.177	28.16	325.0	64.0	59.9	0.82	0.94	0.01
SAG24	01,02	h 50 .046,.019,.005	48.134	-71.199	29.23	325.0	57.2	69.8	0.98	0.90	0.01
SAG25	none	h 0 .070	48.089	-71.150	29.85	325.0	73.6	61.0	0.96	0.91	0.01
SAG26	none	h 33 .070	48.078	-71.135	29.97	325.0	63.0	55.2	0.93	0.99	0.01
SAG27	01,02	h 10 .060,.007,.003	48.075	-71.143	28.71	325.0	56.4	73.1	0.77	0.94	0.01
SAG28	01	h 50 .069,.001	48.080	-71.171	26.61	325.0	56.4	63.6	0.76	0.86	0.01
SAG29	01	h 50 .069,.001	48.133	-71.199	29.15	325.0	61.8	73.3	0.92	0.85	0.01
SAG30	01,02,03,04	h 50 .046,.011,.002,.004,.006	48.090	-71.164	28.14	325.0	59.4	63.8	0.94	0.82	0.01
SAG31	01,02,03,04,05	h 20 .035,.008,.003,.003,.010,.011	48.108	-71.154	31.35	325.0	62.7	68.3	0.88	0.99	0.01
SAG32	01,02,03,04	h 25 .038,.007,.002,.013,.010	48.066	-71.128	29.36	325.0	64.1	70.8	0.89	0.98	0.01
SAG33	01,02	h 10 .043,.003,.024	48.100	-71.168	28.62	325.0	73.6	66.7	0.81	0.81	0.01
SAG34	01	h 33 .057,.013	48.119	-71.187	28.76	325.0	74.4	57.9	0.98	0.94	0.01
SAG35	01,02,03	h 10 .056,.001,.004,.009	48.075	-71.147	28.01	325.0	66.2	59.6	0.96	0.83	0.01
SAG36	none	h 33 .070	48.131	-71.176	31.06	325.0	56.6	74.7	0.80	0.84	0.01
SAG37	01,02,03,04	h 50 .036,.010,.008,.009,.006	48.141	-71.177	32.21	325.0	57.9	57.8	0.75	0.86	0.01
SAG38	01,02,03	h 33 .052,.011,.001,.006	48.101	-71.162	29.57	325.0	60.4	59.2	0.83	0.97	0.01
SAG39	01	h 50 .066,.004	48.125	-71.174	30.60	325.0	55.2	65.3	0.81	0.99	0.01
SAG40	none	h 50 .070	48.074	-71.141	28.59	325.0	66.5	60.6	0.97	0.94	0.01
SAG41	01,02,03,04,05	h 20 .048,.009,.002,.002,.004,.005	48.072	-71.135	29.28	325.0	67.6	67.6	0.84	0.96	0.01
SAG42	01,02,03,04	h 0 .053,.003,.003,.004,.007	48.137	-71.193	30.91	325.0	69.8	74.7	0.95	0.87	0.01
SAG43	01,02	h 10 .046,.007,.017	48.123	-71.173	31.00	325.0	63.1	64.3	0.88	0.93	0.01
SAG44	01	h 0 .069,.001	48.087	-71.166	27.83	325.0	55.7	57.7	0.84	0.94	0.01
SAG45	01	h 10 .051,.019	48.117	-71.173	31.16	325.0	73.5	63.6	0.80	0.93	0.01
SAG46	01,02,03,04	h 25 .057,.007,.003,.002,.001	48.122	-71.195	27.84	325.0	71.3	58.4	0.99	0.95	0.01
SAG47	01,02	h 50 .051,.013,.006	48.093	-71.146	31.07	325.0	69.2	61.0	0.83	0.84	0.01
SAG48	01,02	h 25 .054,.013,.003	48.117	-71.184	29.06	325.0	64.6	57.0	0.79	0.98	0.01
SAG49	01,02,03,04	h 10 .053,.006,.007,.002,.002	48.102	-71.167	29.18	325.0	66.9	66.4	0.95	0.92	0.01
SAG50	01,02,03	h 20 .046,.006,.007,.010	48.069	-71.136	28.77	325.0	63.5	63.5	0.97	0.95	0.01
SAG51	01,02,03	h 0 .053,.008,.001,.008	48.070	-71.138	28.43	325.0	71.0	63.0	0.80	0.90	0.01
SAG52	01	h 10 .068,.002	48.121	-71.203	27.54	325.0	57.9	69.2	0.82	0.94	0.01
SAG53	01,02,03,04	h 50 .052,.005,.003,.007,.003	48.131	-71.212	27.52	325.0	61.8	70.0	0.79	0.88	0.01
SAG54	01,02	h 25 .049,.017,.004	48.080	-71.163	27.25	325.0	57.6	60.3	0.91	0.83	0.01

SAG55	01,02,03,04	h 25 .051,.006,.004,.006,.003	48.091	-71.146	30.87	325.0	70.2	65.0	0.91	0.87	0.01
SAG56	01,02,03,04,05	h 25 .049,.005,.007,.006,.002,.001	48.075	-71.152	27.68	325.0	60.3	61.9	0.77	0.95	0.01
SAG57	01,02,03	h 33 .053,.011,.005,.001	48.134	-71.185	30.76	325.0	60.4	74.9	0.81	0.92	0.01
SAG58	01,02	h 33 .026,.022,.022	48.113	-71.174	30.13	325.0	73.2	56.9	0.92	0.85	0.01
SAG59	01,02,03	h 10 .061,.001,.002,.005	48.122	-71.171	30.56	325.0	55.1	72.6	0.88	0.93	0.01
SAG60	01	h 10 .058,.012	48.082	-71.147	28.95	325.0	70.5	59.9	0.83	0.99	0.01
SAG61	01	h 20 .048,.022	48.136	-71.198	30.11	325.0	72.5	69.4	0.95	0.97	0.01
SAG62	01	h 50 .064,.006	48.093	-71.163	28.49	325.0	65.1	66.0	0.90	0.97	0.01
SAG63	01,02,03	h 0 .046,.003,.006,.015	48.129	-71.190	30.28	325.0	73.1	60.5	0.86	1.00	0.01
SAG64	01,02,03,04	h 50 .040,.011,.007,.010,.001	48.080	-71.152	28.08	325.0	65.6	68.0	0.93	0.90	0.01
SAG65	01,02,03,04	h 20 .042,.015,.005,.007,.001	48.098	-71.133	31.94	325.0	57.3	56.8	0.88	0.94	0.01
SAG66	01,02,03,04	h 25 .043,.004,.013,.008,.003	48.109	-71.152	31.23	325.0	57.9	63.7	0.90	0.82	0.01
SAG67	01,02	h 33 .063,.003,.004	48.090	-71.136	31.04	325.0	59.7	56.3	0.89	0.91	0.01
SAG68	01	h 33 .063,.007	48.085	-71.160	27.45	325.0	69.5	67.1	0.93	0.87	0.01
SAG69	none	h 0 .070	48.129	-71.209	27.66	325.0	60.3	72.2	0.84	0.96	0.01
SAG70	01,02,03	h 10 .050,.011,.006,.003	48.093	-71.150	29.85	325.0	58.6	68.2	0.99	0.83	0.01
SAG71	none	h 20 .070	48.145	-71.208	29.90	325.0	69.7	65.5	0.78	0.90	0.01
SAG72	none	h 20 .070	48.110	-71.183	27.93	325.0	70.4	67.6	0.98	0.81	0.01
SAG73	01,02,03,04	h 10 .055,.000,.005,.003,.007	48.106	-71.170	29.23	325.0	66.4	71.9	0.80	0.98	0.01
SAG74	01,02	h 20 .050,.003,.016	48.076	-71.149	28.13	325.0	61.6	61.6	0.84	0.87	0.01
SAG75	none	h 20 .070	48.084	-71.143	30.44	325.0	75.0	71.5	0.99	0.85	0.01
SAG76	none	h 25 .070	48.140	-71.200	29.98	325.0	61.1	65.2	0.80	0.80	0.01
SAG77	01	h 0 .065,.005	48.083	-71.132	31.37	325.0	67.6	59.4	0.88	0.83	0.01
SAG78	01,02,03,04,05	h 0 .045,.007,.003,.008,.002,.004	48.118	-71.192	28.24	325.0	62.9	66.4	0.94	0.81	0.01
SAG79	01,02	h 0 .057,.005,.008	48.095	-71.126	32.20	325.0	55.6	58.9	0.76	0.93	0.01
SAG80	01,02	h 50 .067,.001,.002	48.131	-71.199	28.95	325.0	61.7	67.6	0.94	0.81	0.01
SAG81	01,02,03,04	h 10 .042,.014,.011,.002,.001	48.126	-71.179	31.26	325.0	68.4	56.7	0.80	0.99	0.01
SAG82	01,02,03,04	h 20 .039,.005,.008,.013,.005	48.121	-71.171	31.08	325.0	63.1	68.3	0.97	0.87	0.01
SAG83	01,02,03	h 10 .028,.002,.019,.020	48.082	-71.131	32.52	325.0	74.3	61.7	0.82	0.96	0.01
SAG84	01,02,03	h 20 .060,.007,.001,.002	48.116	-71.172	30.01	325.0	57.1	74.3	0.77	0.83	0.01
SAG85	01,02	h 50 .057,.009,.004	48.114	-71.169	31.01	325.0	69.3	61.9	0.76	0.96	0.01
SAG86	01,02	h 25 .061,.002,.006	48.071	-71.134	29.42	325.0	71.0	56.0	0.86	0.87	0.01
SAG87	01,02	h 20 .064,.002,.004	48.104	-71.182	27.20	325.0	68.2	59.5	0.75	0.93	0.01
SAG88	01,02	h 10 .053,.006,.011	48.116	-71.180	29.53	325.0	72.3	66.2	0.88	0.88	0.01
SAG89	01,02	h 0 .045,.014,.011	48.104	-71.168	29.22	325.0	55.2	68.2	0.90	0.85	0.01
SAG90	01	h 0 .058,.012	48.135	-71.177	31.60	325.0	58.6	72.6	0.98	0.97	0.01
SAG91	01,02,03,04,05	h 33 .041,.002,.014,.005,.005,.003	48.086	-71.128	31.27	325.0	57.4	61.6	0.76	0.94	0.01
SAG92	none	h 50 .070	48.102	-71.175	28.14	325.0	63.2	74.7	0.80	0.98	0.01
SAG93	01,02,03	h 10 .060,.003,.005,.003	48.125	-71.191	29.20	325.0	70.3	64.6	0.87	0.87	0.01
SAG94	01,02	h 25 .065,.001,.005	48.132	-71.211	27.28	325.0	67.3	72.3	0.77	0.90	0.01
SAG95	01,02,03,04,05	h 50 .048,.002,.005,.004,.008,.002	48.103	-71.162	30.47	325.0	74.4	74.9	0.79	0.82	0.01
SAG96	01,02	h 50 .057,.009,.004	48.123	-71.185	29.64	325.0	63.6	62.9	0.84	0.99	0.01
SAG97	01,02	h 50 .067,.001,.002	48.130	-71.193	29.64	325.0	67.4	65.7	0.95	0.85	0.01
SAG98	01,02,03,04,05	h 33 .051,.010,.001,.001,.004,.002	48.069	-71.130	29.46	325.0	65.0	64.3	0.97	0.84	0.01
SAG99	01,02	h 10 .063,.004,.003	48.096	-71.177	27.65	325.0	55.3	56.1	0.84	0.92	0.01
SAG*0	01,02,03,04	h 10 .023,.008,.030,.006,.002	48.111	-71.159	31.57	325.0	66.2	59.4	0.93	0.99	0.01